Cumhuriyet Sci. J., 46(1) (2025) 142-151
DOI: https://doi.org/10.17776/csj.1525584

Cumhuriyet Science Journal

| csj.cumhuriyet.edu.tr | Founded: 2002 ISSN: 2587-2680 e-ISSN: 2587-246X Publisher: Sivas Cumhuriyet University

Kinetics of the Mixed Spin (1, 3/2) Ising Model in the Presence of an Oscillating Magnetic Field by Using the Path Probability Method

Mustafa Gençaslan [1,a,*], Abdulrahman Mohammed Kaif Awwadee [1,b]

[1] *Department of Physics, Erciyes University, Kayseri, Türkiye.*
**Corresponding author*

Research Article

History
Received: 31/07/2024
Accepted: 12/01/2025

ABSTRACT

Kinetics of the mixed spin (1, 3/2) Ising ferrimagnetic system on the two interpenetrating square lattices with the bilinear and crystal-field interactions under an oscillating magnetic field were investigated by using the path probability method (PPM). We examined time variations in average dynamic magnetizations and obtained phases and then we investigated the thermal behaviors of dynamic magnetizations to determine the nature of the dynamic phase transitions and find their temperature values. We also constructed the dynamic phase diagrams in (d,T) and (h_0,T) planes. Dynamic phase diagrams display the paramagnetic (p), ferrimagnetic (i), and mixed phases (i+p), and one dynamic tricritical point and dynamic double critical endpoints. We found that the PPM is a more convenient method to investigate the kinetics and dynamics behaviors of ferrimagnetism.

Keywords: Mixed spin-1 and spin- 3/2 Ising system, Path probability method, Dynamic phase transition temperatures, Dynamic magnetic phase diagrams.

[a] *gaslan@erciyes.edu.tr* *https://orcid.org/0000-0002-5726-1733* [b] *abd.m.kaif@gmail.com* *https://orcid.org/0009-0009-7377-7877*

Introduction

The usage areas of molecular-based magnetic materials in today's technology are increasing. Therefore, both theoretical and experimental studies on understanding the magnetic properties of these materials have increased and will continue to increase. Since it is essential to understand the equilibrium and nonequilibrium phase behaviors of these materials, many different theoretical models and methods have been developed in this context, the different Ising spin systems being the origin of most of them, and it has been observed that mixed spin systems give better results than the pure spin system. The mixed spin (1, 3/2) Ising system is one of the most practical prototype system to investigate molecular-based magnetic materials, such as $[NiCr_2(bipy)_2(C_2O_4)_4(H_2O)]H_2O$ [1], Fe_4N [2], and $[Co(hfac)_2]BNO^*$ [3]. Moreover, the system also gives interesting hysteresis loop behavior and rich equilibrium and nonequilibrium critical phenomena. Equilibrium behaviors of the system were studied by using the mean-field theory, the effective-field theory, the renormalization group theory, Green's function technique, Monte Carlo simulations, etc., (see [4-8] and references therein). The system was also used to investigate nanomaterials' thermal and magnetic properties, such as nanowires, nanotubes, and nanoislands [9-12].

On the other hand, less work was performed on the dynamic behaviors of the system. Keskin and co-workers conducted one of the earlier works [13, 14]. They determined the dynamic phase transition [13] and dynamic compensation temperatures using the dynamic mean field approximation (DMFA) and presented the dynamic phase diagrams [14]. The dynamic magnetic properties of the Fe_4N compound structure were investigated by Kantar and Ertaş [2] using the DMFA, and by Shi and Qi [15] using the dynamic effective field theory (DEFT). Also, Ertaş and Keskin [16] investigated the dynamic hysteresis and dynamic compensation temperatures of the system using the DEFT. The dynamic magnetic behavior of double-walled nanotubes was investigated by Benhouria et al., using the dynamic Monte Carlo simulations (DMCs) [18]. The path probability method (PPM) [27] used in the present paper has been very popular in Ising-like systems in recent years. While other methods include only one rate constant, the PPM includes two rate constants, one of which (k_2) corresponds to the wheel speed in the melt spinning technique in the rapid solidification process. (2) Even in the simplest use of the Hamiltonian, the order parameters become coupled. (3) The derivation of the dynamic equations is easier and more systematic than the other methods. Therefore, the application area of this method is quite wide. With the motivation of this information, Gençaslan and co-workers used the PPM to various mixed spin Ising ferrimagnetic systems (IFSs) in the presence of an oscillating magnetic field applied on different crystal fields to investigate the dynamic magnetic properties of molecular-based magnetic materials, namely dynamic hysteresis loops behaviors [19-24] and the dynamic phase diagrams (DPDs) [24-30]. They reported some interesting and rich dynamic phase diagram behaviors and dynamic hysteresis loop behaviors.

In this study, we investigate the dynamic phase transition temperatures (DPTs) and DPDs of the mixed spin (1, 3/2) IFS with the bilinear (*J*) and crystal field interactions (*D*) under a time-varying magnetic field (sinusoidal) by using the PPM. Moreover, we give the time variations of average dynamic magnetizations for different system parameters. After Section 2, where the model and derivations of dynamic equations are presented, the results and discussion are given in Section 3. Finally, concluding remarks are presented in Section 4.

Model and Derivation of Dynamic Equations

As depicted in Fig. 1, the mixed spin-1 and spin-3/2 IFS are defined on two square lattices with interpenetrating sublattices *A* and *B*. Sublattice *A* have spin values $\sigma_i^A = \pm 1,0$, sublattice *B* have spin values $S_j^B = \pm_{2,\pm\frac{1}{2}}^{3}$.

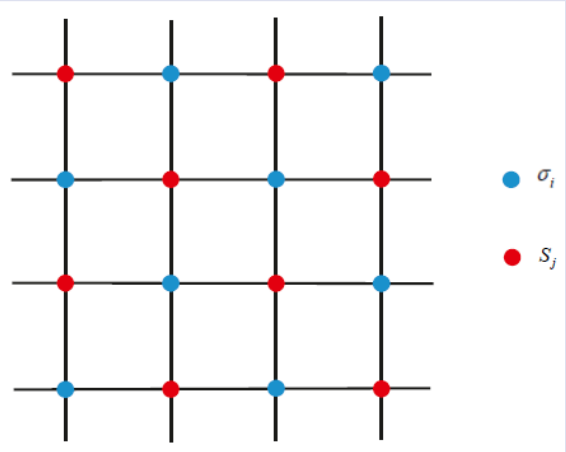

Figure 1. (Color online) The schematic representation of the two interpenetrating square lattices. The lattice is filled by σ_i (solid blue circles) and S_j (solid red circles) spins. J is the exchange couplings between the nearest-neighbor pairs of spins $\sigma_i - S_j$.

Hamiltonian of the system with bilinear (*J*) nearest-neighbor pair interaction and a crystal field interaction (*D*), under the presence of a sinusoidal magnetic field is written as

$$\mathcal{H} = -J\sum_{(i,j)}\sigma_i^A S_j^B + D\sum_i[(3\sigma_i^A)^2 - 2] + D\sum_j[(S_j^B)^2 - \tfrac{5}{4}] - H(\sum_i \sigma_i^A + \sum_j S_j^B) \quad (1)$$

where $< i,j >$ on the sublattices imply a summing of all nearest-neighboring sites. $H$is a sinusoidal magnetic field with amplitude H_0 and the angular frequency $\omega = 2\pi\nu$, thus $H = H_0\cos(\omega t)$.

The system has the following five order parameters: (1) The average magnetization or the dipole moment$m^A =< \sigma_i^A >$, (2) the quadrupole moment, $q^A = 3 < (\sigma_i^A)^2 > -2$, for *A* sublattice and (3) The dipole moment or average magnetization $m^B =< S_j^B >$, (4) the quadrupole moment, $q^B =< (S_j^B)^2 > -\frac{5}{4}$, and (5) the octupole moment, $r^B = \frac{5}{3} < \left(S_j^B\right)^3 > -\frac{41}{12} < S_j^B >$, for *B* sublattice.

Since the formulation is given and discussed in Refs. [23, 24] in detail, we will briefly summarize it here. At this stage, the set of coupling average dynamic equations for order parameters can be obtained by using Eqs. (2)-(7) in Ref. [23] as

$$\begin{aligned}\Omega\frac{dm^A}{d\xi} = \{&[\frac{1}{2}(sinh(2b) - cosh(2b))k_1 + (sinh(a-b) - cosh(a-b) - sinh(a+b)\\ &- cosh(a+b))k_2 + \frac{1}{2}(sinh(2b) - cosh(2b))k_3]m^A\\ &+\frac{1}{6}[(sinh(2b) - cosh(2b) - 2\,cosh(a+b) - 2\,sinh(a+b))k_1 + 2(sinh(a+b)\\ &+ cosh(a+b) + sinh(a-b) - cosh(a-b))k_2 + (cosh(2b) - sinh(2b)\\ &+2\,cosh(a-b) - 2\,sinh(a-b))k_3]q^A\\ &+(\frac{1}{3}k_1 + \frac{2}{3}k_2)\,cosh(a+b) + (\frac{1}{3}k_1 + \frac{2}{3}k_2)\,sinh(a+b) - (\frac{2}{3}k_2 + \frac{1}{3}k_3)\,cosh(a-b)\\ &+(\tfrac{2}{3}k_2 + \tfrac{2}{3}k_3)\,sinh(a-b) - (\tfrac{1}{3}k_1 + \tfrac{1}{3}k_3)\,cosh(2b) + (\tfrac{1}{3}k_1 - \tfrac{1}{3}k_3)\,sinh(2b)\}/[ke^b(cosh(a) + e^{-3b})],\end{aligned} \quad (2)$$

$$\begin{aligned}\Omega\frac{dq^A}{d\xi} = &\{\frac{3}{2}[(sinh(2b) - cosh(2b))k_1 + (cosh(2b) - sinh(2b))k_3]m^A\\ &+[\frac{1}{2}(sinh(2b) - cosh(2b) - 2\,cosh(a+b) - 2\,sinh(a+b))k_1\\ &+(\tfrac{1}{2}(sinh(2b) - cosh(2b) - 2\,cosh(a-b) + 2\,sinh(a-b))k_3]q^A\\ &+k_1(cosh(a+b) + cosh(a+b)) + k_3(cosh(a-b) - sinh(a-b)\\ &+(k_1 + k_3)\,sinh(2b) - (k_1 + k_3)\,cos(2b)\}/[ke^b(cosh(a) + e^{-3b})]\end{aligned} \quad (3)$$

and

$$\Omega\frac{dm^B}{d\xi} = \{-\frac{1}{5}[(2\sqrt{k_1k_2}+9k_2-k_1)\,cosh(a)e^c-(6\sqrt{k_1k_2}+k_2+3k_1)\,cosh(b)e^{-c}]m^B$$
$$+\tfrac{1}{2}[(2\sqrt{k_1k_2}-k_2-k_1)\,sinh(b)e^{-c}-(2\sqrt{k_1k_2}-3k_2+k_1)\,sinh(a)]e^c]q^B \quad (4)$$
$$+\frac{1}{5}[(2\sqrt{k_1k_2}-3k_2+k_1)\,cosh(b)e^{-c}-3(2\sqrt{k_1k_2}-k_2-k_1)\,cosh(a)e^c]r^B$$
$$+\tfrac{1}{2}[(2\sqrt{k_1k_2}+k_2-k_1)\,sinh(b)e^{-c}+(2\sqrt{k_1k_2}+3k_2+k_1)\,sinh(a)e^c]\}/2k[cosh(a)e^c+cosh(b)e^{-c}],$$

$$\Omega\frac{dq^B}{d\xi} = \{\frac{1}{5}(\sqrt{k_1k_2}-k_1)[6\,sinh(b)e^{-c}-2\,sinh(a)e^c]m^B$$
$$-(\sqrt{k_1k_2}+k_1)[cosh(a)e^c+cosh(b)e^{-c}]q^B \quad (5)$$
$$+\frac{2}{5}(\sqrt{k_1k_2}-k_1)[3\,sinh(a)e^c+sinh(b)e^{-c}]r^B$$
$$+(\sqrt{k_1k_2}+k_1)[cosh(a)e^c-cosh(b)e^{-c}]\}/2k[cosh(a)e^c+cosh(b)e^{-c}],$$
$$\Omega\frac{dr^B}{d\xi} = \{\tfrac{1}{5}[(\sqrt{k_1k_2}-3k_2+2k_1)\,cosh(a)e^c+3(\sqrt{k_1k_2}+k_2-2k_1)\,cosh(b)e^{-c}]m^B$$
$$+\tfrac{1}{2}[(\sqrt{k_1k_2}+k_2-2k_1)\,sinh(a)e^c-(\sqrt{k_1k_2}-3k_2+2k_1)\,sinh(b)e^{-c}]q^B \quad (6)$$
$$-\frac{1}{5}[(3\sqrt{k_1k_2}+k_2+6k_1)\,cosh(a)e^c-(\sqrt{k_1k_2}-9k_2-2k_1)\,cosh(b)e^{-c}]r^B$$
$$-\tfrac{1}{2}[(\sqrt{k_1k_2}-k_2-2k_1)\,sinh(a)e^c+(\sqrt{k_1k_2}+3k_2+2k_1)\,sinh(b)e^{-c}]\}/2k[cosh(a)e^c+cosh(b)e^{-c}],$$

where $h=\frac{H}{Jz}$, $d=\frac{D}{Jz}$, $T=(\beta Jz)^{-1}$, $k=\frac{k_1}{k_2}$, $k_3=\sqrt{k_1k_2}$, $\xi=\omega t$, $z=4$, and $\frac{a=(m^B+h_0\,cos\,\xi)}{T}$, $b=\frac{d}{T}$in the Eqs. (2, 3), and $a=\frac{3}{2}(m^A+h_0\,cos\,\xi)/T$, $b=\frac{1}{2}(m^A+h_0\,cos\,\xi)/T$and $c=\frac{d}{T}$ in the Eqs. (4-6). It is worth remembering here that k_1 and k_2 are the rate constants that emerge as an advantage of the PPM. In the PPM, the rate constant k_1 corresponds to spin particle translation, i.e. the insertion or removal of particles across the lattices, and k_2 relates to spin particle rotation at a given site, and k_3 corresponds to spin translation and rotation at the same time. Using the geometric mean, $k_3$can be expressed in terms of k_1 and k_2 as $k_3=\sqrt{k_1k_2}$. It is expected that two particles cannot be inserted, removed, or rotated at the same time. These constants for sublattices *A* and *B* are given in Table I. In the present paper, we fixed $k_1=1.0$ in all numerical calculations.

Table I. The description of rate constants for the *A* and *B* sublattices

		1	0	-1
A sublattice	1		k_1	k_2
	0	k_1		k_1
	-1	k_2	k_1	

		+3/2	+1/2	-1/2	-3/2
B sublattice	+3/2		k_1	k_3	k_2
	+1/2	k_1		k_2	
	-1/2	k_3	k_2		k_1
	-3/2	k_2	k_3	k_1	

We numerically solved these equations by combining the numerical methods of the Romberg integration with the Adams-Moulton predictor-corrector, for a given set of system parameters and initial values. The obtained results and their discussion will be presented in the next section. Since $m^A$and m^B determine the dynamic magnetic properties of the system, we are only interested in the behaviors of $m^A$and m^B. Moreover, the total magnetization is defined as $m^T=\frac{(m^A+m^B)}{2}$.

Time Variations in Average Dynamic Magnetizations

To find phases occurring in the system, we examine the stationary solutions of average magnetizations ($m^A$and m^B), i.e., Eqs. (2) and (4). The stationary solutions of Eqs. (2) and (4) are periodic functions of ξ with period 2π, i.e.,

$$m^{A,B}(\xi+2\pi)=m^{A,B}(\xi) \quad (7)$$

Furthermore, they can be one of two solutions according to whether they have or do not have the following condition

$$m^{A,B}(\xi + \pi) = -m^{A,B}(\xi) \quad (8)$$

It is one of the solutions that satisfies Eq. (8), which is called the symmetrical solution and expresses a paramagnetic (p) phase. In this case, $m^A$and m^B oscillate around zero as seen in Fig. 2(a). The other solution does not satisfy Eq. (8), which is called the nonsymmetric solution, corresponds to a ferrimagnetic (i) phase. For this reason, m^A oscillates around ± 1 and m^Baround ±3/2, as exhibited in Fig. 2(b). The i and p phases are fundamental phases. We found one mixed phase, i.e., p+i where the p and i phases coexist, displayed in Fig. 2(c). We also investigated the effect of rate constants on stationary solutions of $m^A$and m^B, and we observed the system rapidly relaxes to the p phases while k_2 values increase, as seen in Fig. 3. We should mention that since most systems have a longer relaxation time for a rotation (k_2) than for a translation (k_1), we took $k_2 > k_1$ in numerical

calculations. Figs. 2 and 3 exhibit the solutions of $m^A$and $m^B$with different initial values, with the same color code. If examined carefully, it is seen that the solutions given as Fig. 2(a) and Fig. 3 are independent of initial values, while the those given as Figs. 2 (b)-(c) are dependent on the initial values. If we look at Fig. 2(a) carefully, we see that $m^A$and m^Boscillate around zero, which is understood to represent the paramagnetic phase (p). In Fig. 2(b), $m^A$and m^Boscillate exactly around ± 1 and $\pm\frac{3}{2}$, that is, they show the ferrimagnetic (i) phase. The mixed or hybrid phase (p + i) behavior, that is, $m^A$and m^Boscillate exactly $\pm 1, \pm\frac{3}{2}$and also around zero, is clearly seen in Fig. 2(c). While the oscillations in the calculations found with the mean field approximation for the same mixed spin system in Refs. [2, 14] occur around approximate values, it is interesting that the oscillations obtained with the PPM in the present study occur exactly around 0, ± 1, $\pm\frac{3}{2}$ as expected. Fig. 3(a)-(d) shows the effect of the changing rate constant on the paramagnetic phase while all system parameters remain the same. It is seen that the system reaches the paramagnetic phase more quickly as the rate constant parameter k_2 increases.

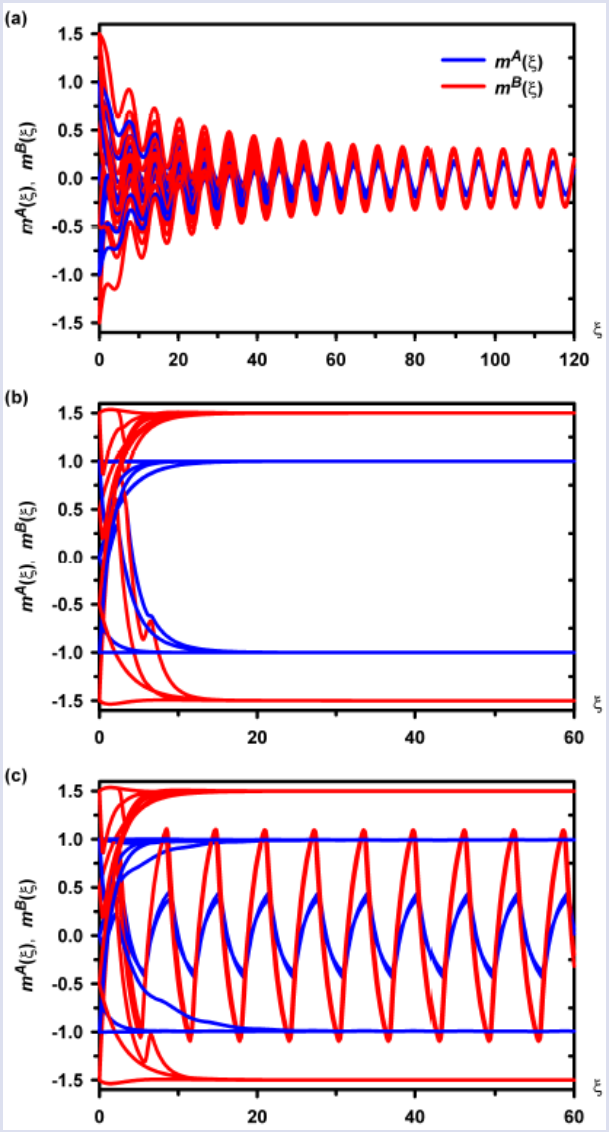

Figure 2. (Color online) Time variations of the magnetizations ($m^A$and m^B), with $d = 4.0$, $k_1 = 1.0$and$k_2 = 1.0$. (a) Exhibiting a paramagnetic (p) phase for $T = 1.50$, $h_0 = 0.350$; (b) Illustrating a ferrimagnetic (i) phase for $T = 0.10$, $h_0 = 0.60$; (c) Displaying a mixed or coexistence phase, namely the i+p phase for $T = 0.75$, $h_0 = 0.60$.

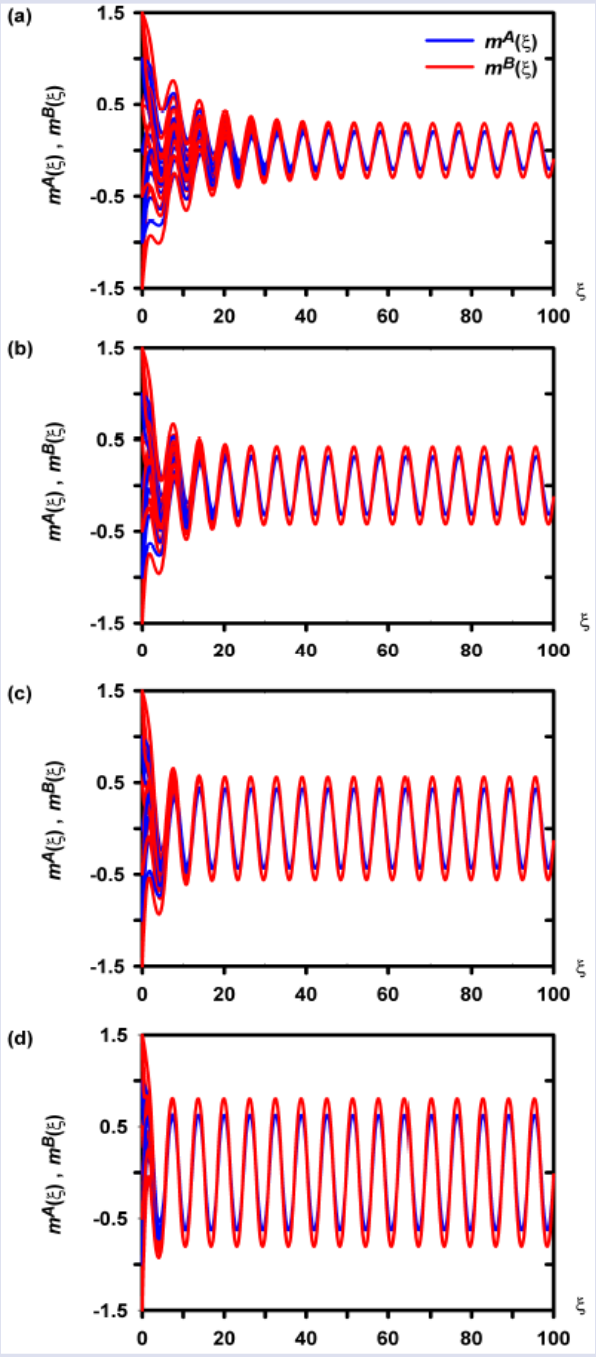

Figure 3. (Color online) Time variations of the magnetizations ($m^A$and m^B) for only paramagnetic (p) phase for$T = 1.40$, $d = 0.25$, $h_0 = 0.60$, $k_1 = 1.0$and four different values of k_2. (a) $k_2 = 2.0$, (b)$k_2 = 2.5$, (c) $k_2 = 3.0$ and (d)

Dynamic Phase Transition Temperatures (DPTs)

Dynamic phase transition temperatures (DPTs) are obtained by investigating the thermal behavior of dynamic magnetizations that are given as [31]

$$M^{A,B} = \frac{1}{2\pi}\int_0^{2\pi} m^{A,B}(\xi)\, d\xi. \quad (9)$$

As we mentioned before, since $m^A$and m^Bdetermine the dynamic magnetic properties of the system, we only need to examine the behaviors of $M^A$and M^B. The solutions of Eq. (9) give us to whether a first or second order phase transition occurs and the temperature values of these transitions. Firstly, we numerically solved Eq. (9) for$d = 4.0, k_1 = 1.0, k_2 = 2.0$, and various values$h_0$, and obtained the thermal behavior of dynamic magnetizations ($|M^A|$and $|M^B|$) as seen in Fig. 4. Hence, Fig. 4 (a) is presented for$h_0 = 0.35$. Fig. 4(a) exhibits that $M^{A,B}$ decreases to zero continuously as *T* increases. Therefore, the system undergoes a second-order phase transition at $T_C = 1.40$ and the dynamic transition is from the *i* phase to the *p* phase, for all initial values of $|M^A|$and $|M^B|$. This fact is very clearly seen in Fig. 6 (c) for $h_0 = 0.35$. Fig. 4(b) is plotted for $h_0 = 0.60$, and it displays that $M^{A,B}$ firstly the *p* phase up to $T_t = 0.075$ for the initial values of $|M^A| = 0.0$, it exhibiting the *i* phase for the $|M^A| = 1.0$; $|M^B| = 0.5, 1.5$ up to $T_C = 1.16$. They are exhibiting two successive phase transitions, namely (b_1) illustrating a first-order phase transition at $T_t = 0.075$, and $(b_2 b_2)$ displaying a second-order phase transition at $T_C = 1.16$. Thus, the *i*+*p* mixed phase takes place between T_t and T_C. Fig. 4(c) is constructed for $h_0 = 0.80$; (c_1)-(c_4) exhibiting four successive phase transitions, namely the first one is (c_1) at $T_{t1} = 0.08$for initial values $|M^A| = 0.0$; $|M^B| = 0.5$ and $T_{t2} = 0.355$, the second one is (c_2) at $T_{t1} = 0.08$ for initial values $|M^A| = 0.0$; $|M^B| = 1.5$ and $T_{t2} = 0.365$, the third one is (c_3) at $T_{t2} = 0.355$ for initial values $|M^A| = 1.0$; $|M^B| = 0.5$ and finally the fourth one is (c_4) at $T_t = 0.600$ for initial values $|M^A| = 1.0$; $|M^B| = 1.5$. This fact is very clearly seen in Fig. 6 (c) for $h_0 = 0.80$. Thus, the *i*+*p* mixed phase takes place between $T_t = 0.08$ and $T_t = 0.600$.

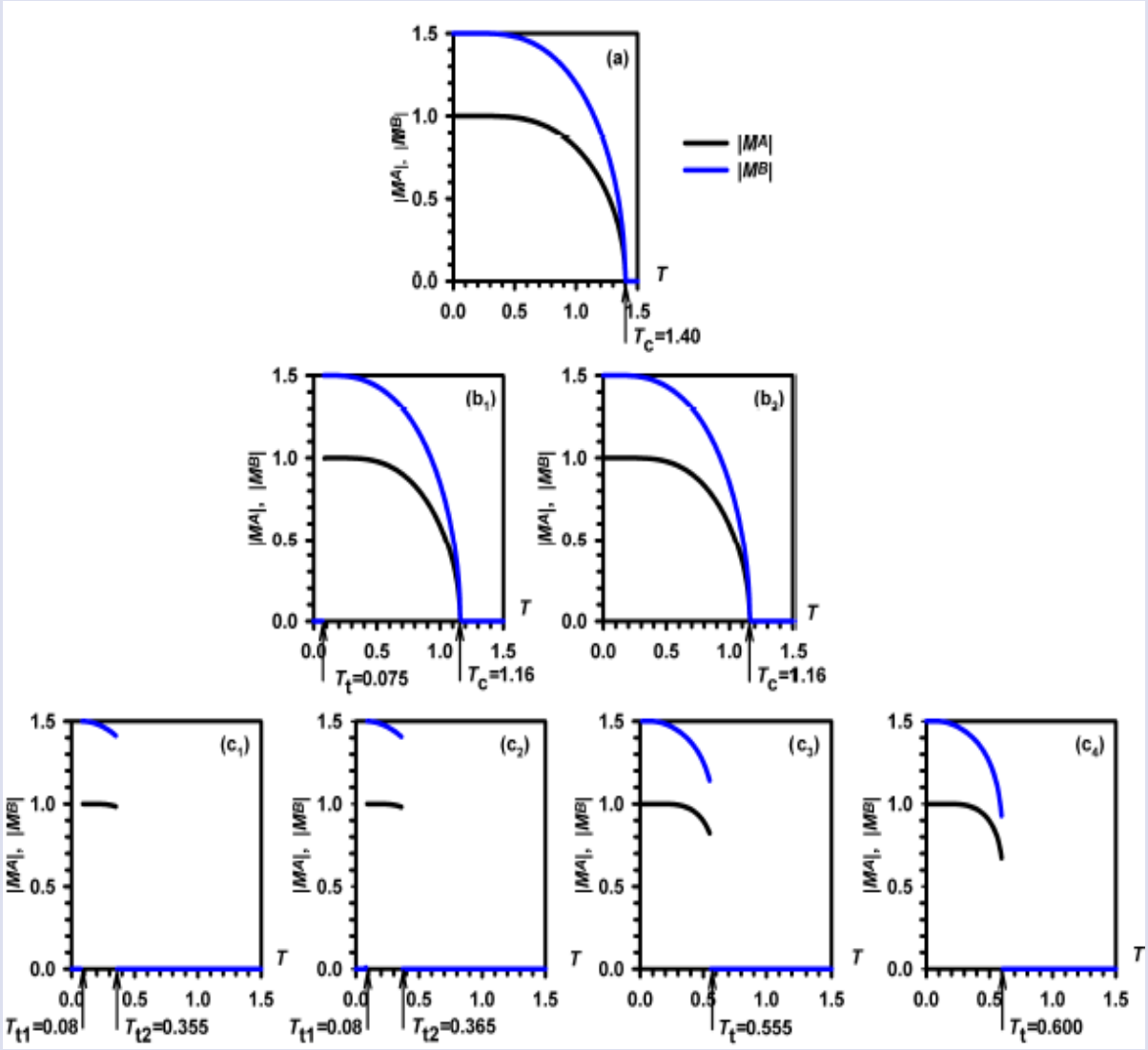

Figure 4. (Color online) The thermal behavior of dynamic magnetizations ($|M^A|$) $T_c$and $T_t$are the second-order and first-order phase transition temperatures for both $|M^A|$and $|M^B|$, respectively, with $d = 4.0$, $k_1 = 1.0, k_2 = 2.0$. (a) Exhibiting a second-order phase transition from the ferrimagnetic (*i*) phase for $T_C = 1.40$, $h_0 = 0.35$, for all initial values of $|M^A|$and $|M^B|$; (b_1) and (b_2) were obtained for $h_0 = 0.60$and two different initial values of $|M^A| = 0.0$; $|M^B| = 0.5, 1.5$ and $|M^A| = 1.0$; $|M^B| = 0.5, 1.5$, respectively, and they are exhibiting two successive phase transitions, namely (b_1) illustrate a first-order phase transition at $T_t = 0.075$, and (b_2) displaying a second-order phase transition at $T_C = 1.16$. For $h_0 = 0.80$, (c_1)-(c_4) exhibiting four successive phase transitions, namely the first one is (c_1) at $T_{t1} = 0.08$ for initial values $|M^A| = 0.0$; $|M^B| = 0.5$ and $T_{t2} = 0.355$, the second one is (c_2) at $T_{t1} = 0.08$ for initial values$|M^A| = 0.0$; $|M^B| = 1.5$ and $T_{t2} = 0.365$, the third one is (c_3) at $T_{t2} = 0.555$ for initial values $|M^A| = 1.0$

To see the nature of the DPT temperatures for the case where$h_0$is fixed but for the crystal-field interaction$d$is varied, we obtained Fig.5 by solving Eq.(9). So that, Fig.5(a) exhibits a second-order phase transition from the ferrimagnetic (*i*) phase for $T_c = 0.765$, $d = 0.10$, for all initial values of $|M^A|$and $|M^B|$. For $d = 1.0$, Fig.5 (b_1)-(b_3) shows three successive phase transitions, namely the first one is (b_1) at $T_t = 0.365$ for initial values $|M^A| = 0.0$; $|M^B| = 0.5, 1.5$, the second one is (b_2) at $T_t = 0.555$ for initial values $|M^A| = 1.0$; $|M^B| = 0.5$, the third one is (b_3) at $T_t = 0.595$ for initial values $|M^A| = 1.0$; $|M^B| = 1.5$. For $d = 6.0$, very similar results were found as presented in Fig.4 (c_1)-(c_4) exhibiting four successive phase transitions, namely the first one is (c_1) at $T_{t1} = 0.130$ for initial values $|M^A| = 0.0$; $|M^B| = 0.5$ and $T_{t2} = 0.355$, the second one is (c_2) at $T_{t1} = 0.130$ for initial values $|M^A| = 0.0$; $|M^B| = 1.5$ and $T_{t2} = 0.365$, the third one is (c_3) at $T_t = 0.555$ for initial values $|M^A| = 1.0$; $|M^B| = 0.5$ and finally the fourth one is (c_4) at $T_t = 0.600$ for initial values $|M^A| = 1.0$; $|M^B| = 1.5$. Thus, the *i+p* mixed phase takes place between $T_{t1} = 0.130$ and $T_t = 0.600$.

Dynamic Phase Diagrams (DPDs)

In the previous section, it was explained how to determine the DPTs, and now we can plot the DPDs in the

(h_0, T) and (d, T) planes for various system parameters, as shown in Figures 6 and 7. In the given DPDs, the dashed and solid lines represent the first- and second-order DPT boundaries, respectively, *TCP* and *B* represent the dynamic triple critical point and the dynamic double critical endpoint [32], respectively. All our calculations were made for$k_1 = 1.0$, $k_2 = 2.0$and various values of $h_0$and d.

Figure 6(a) obtained for $d = 0.25$ in which at low temperature (T) and low values ofh_0, the DPD exhibits ferrimagnetic (*i*), while at high T values displays paramagnetic (*p*) characteristics. The dynamic boundary line separating the *i* and *p* phases is the second-order phase line. There is a region at low T and high h_0 values where the *i* and *p* phases coexist, named the mixed phase (*i+p*). The dynamic first-order phase lines separate the *i+p* phase from the *i* and the *p* phases. Moreover, the system has a dynamic tricritical point (*TCP*) where two first-order phase transition lines merge and transform into a first-order to a second-order phase transition. The DPDs with similar behavior have been reported in various mixed Ising ferrimagnetic systems (see Refs. [27, 33-35] and references therein) and mixed (1, 3/2) IFS [14, 36, 37]. Fig. 6(b) was calculated for $d = 2.50$, which is similar to Fig. 6(a), but the tricritical line becomes shorter and the mixed phase region becomes slightly larger. Additionally, at low temperatures, another mixed phase region appears, terminating in a double critical end point *B*. Fig. 6 (c) and (d) were constructed for $d = 4.0$and$d = 6.0$, respectively. Figures 6 (c) and (d) are quite similar to Fig. 6(b), except for the broadening of the mixed phase region, terminating in a *B*, that occurs at lower temperatures with increasing *d*.

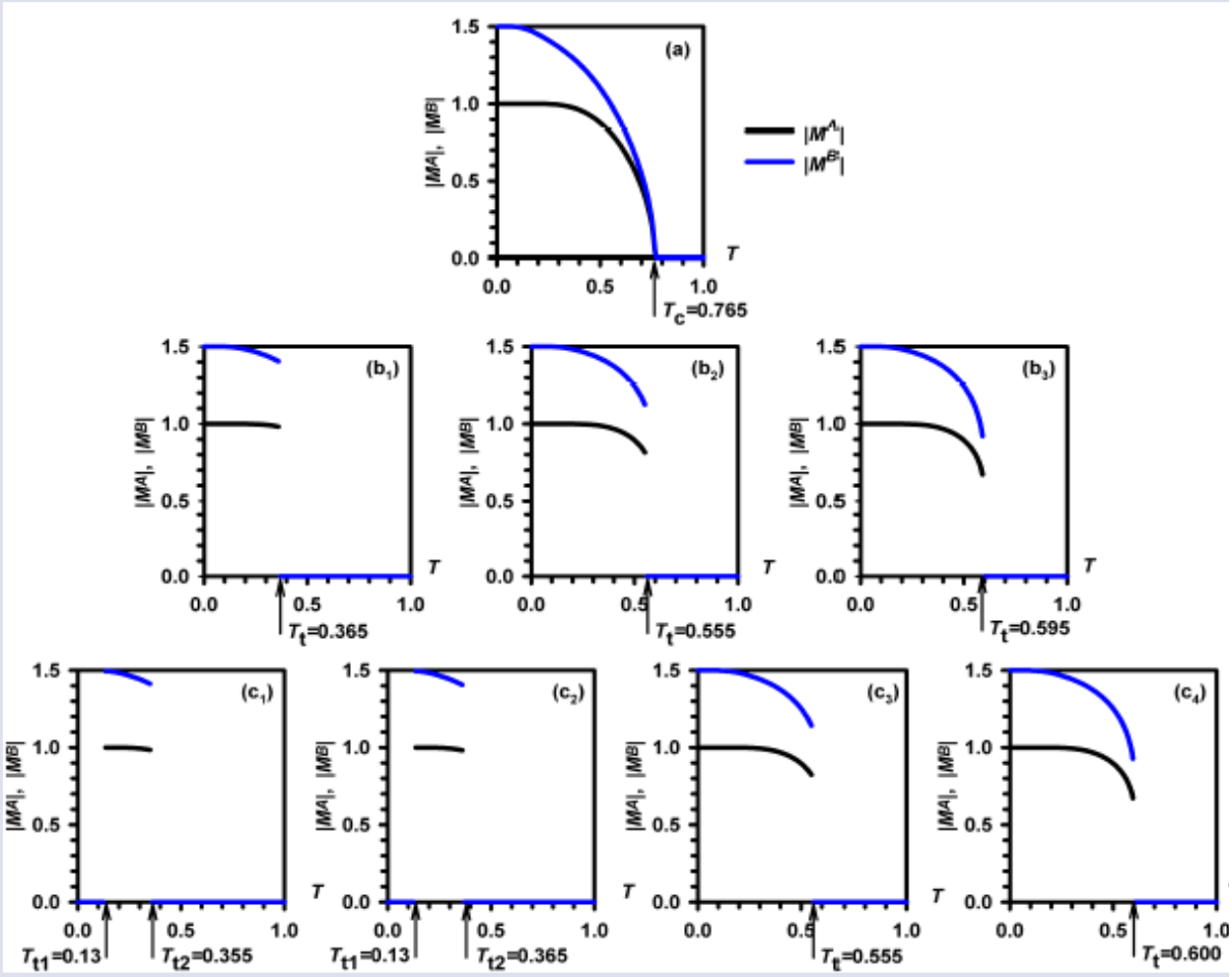

Figure 5.(Color online) The thermal behavior of dynamic magnetizations ($|M^A|$and $|M^B|$) $T_c$and T_t are the second-order and first-order phase transition temperatures for both $|M^A|$and $|M^B|$, respectively, with $d = 4.0$, $k_1 = 1.0, k_2 = 2.0$. (a) Exhibiting a second-order phase transition from the ferrimagnetic (*i*) phase for $T_C = 0.765.$, $d = 0.10$, for all initial values of $|M^A|$and $|M^B|$. For $d = 1.0$, (b_1)-(b_3) exhibiting three successive phase transitions, namely the first one is (b_1) at $T_t = 0.365$ for initial values $|M^A| = 0.0$; $|M^B| = 0.5, 1.5$, the second one is (b_2) at $T_t = 0.555$ for initial values $|M^A| = 1.0$; $|M^B| = 0.5$, the third one is (b_3) at $T_t = 0.595$ for initial values $|M^A| = 1.0$; $|M^B| = 1.5$. For $d = 6.0$found the very similar result were found that (c_1)-(c_4) exhibiting four successive phase transitions, namely the first one is (c_1) at $T_{t1} = 0.130$ for initial values $|M^A| = 0.0$; $|M^B| = 0.5$ and $T_{t2} = 0.355$, the second one is (c_2) at $T_{t1} = 0.130$ for initial values $|M^A| = 0.0$; $|M^B| = 1.5$ and $T_{t2} = 0.365$, the third one is (c_3) at $T_t = 0.555$ for initial values $|M^A| = 1.0$; $|M^B| = 0.5$and finally the fourth one is (c_4) at $T_t = 0.600$ for initial values $|M^A| = 1.0$; $|M^B| = 1.5$.

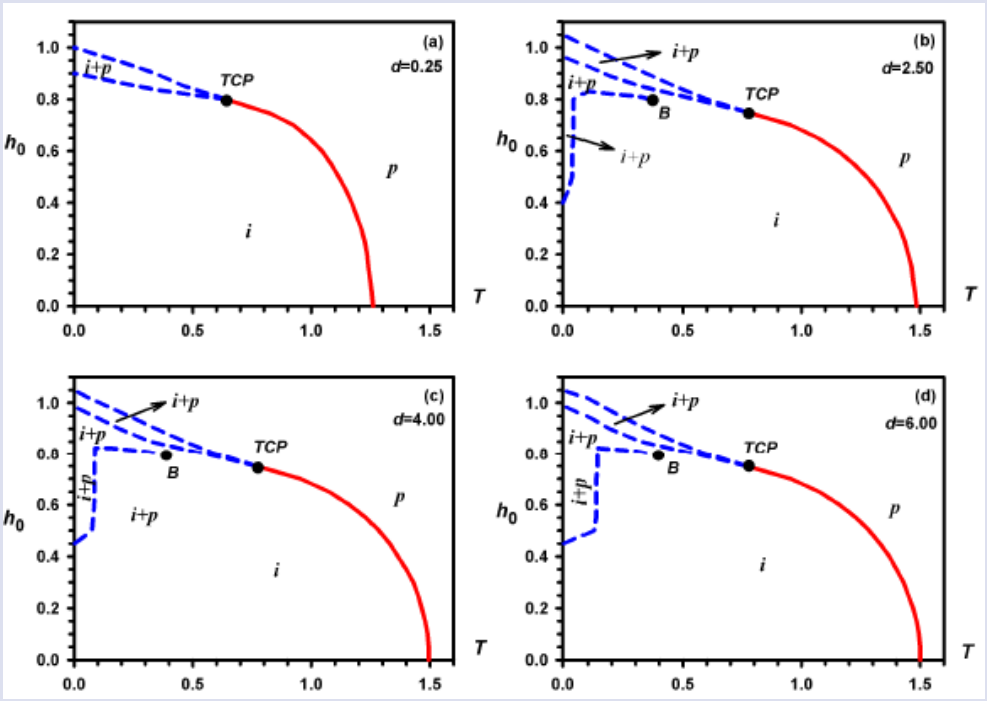

Figure 6. (Color online) The DPDs of the system in the (h_0, T) plane, with $k_1 = 1.0$and$k_2 = 2.0$. The paramagnetic (*p*), ferrimagnetic (*i*), and the *i+p* mixed phase are observed. Solid and dashed lines are the second-order and first-order phase transitions, respectively. The special dynamic critical points are the dynamic tricritical (*TCP*) and the dynamic double critical end (*B*) points. (a) $d = 0.25$, (b) $d = 2.50$, (c) $d = 4.00$, (d) $d = 6.00$.

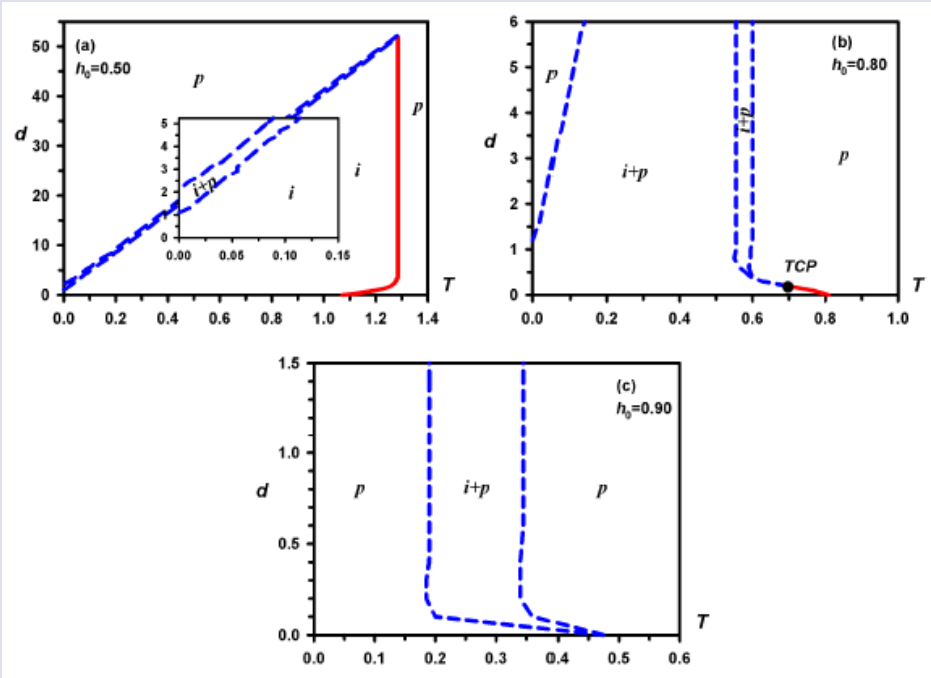

Figure 7. (Color online) The DPDs of the system in the (d, T) plane. It contains *TCP* but not *B*. (a) $h_0 = 0.50$, (b) $h_0 = 0.90$

Fig. 7 exhibits the DPDs in the (d, T) plane for three different values ofh_0. Fig. 7 (a)-(c) are obtained for $h_0 = 0.50; 0.80$ and 0.90 respectively. If one looks carefully at Fig. 7(a), one sees that it contains a very narrow *i+p* mixed phase region that starts at low temperatures and small *d* values, which gradually narrows with increasing *d* values and merges with the second-order phase transition line at high temperatures and large *d* values, i.e. they converge at *TCP* tricritical point. In Figure 7(b), a third dynamic first-order phase transition line appears starting from low temperature and *d* values and goes towards asymptotically high temperature and *d* values. Furthermore, there is also a narrow mixed-phase region, which starts from a *TCP* point at a low *d* value. In Figure 7(c) obtained for $h_0 = 0.90$, a third dynamic first-order phase line and *TCP* point seen in Figure 7(b) disappear, and the *i+p* mixed phase region widens.

Finally, the DPDs we obtained in both the (h_0, T) and the (d, T) plane have a *TCP* point and a dynamic double critical endpoint, and some similar results have been reported in pure [27, 33-35] and mixed spin Ising ferrimagnetic systems [2, 14, 36, 37].

Concluding Remarks

We studied the dynamic phase transition temperatures and dynamic phase diagrams of the mixed spin (1, 3/2) IFS under a sinusoidal magnetic field by using the PPM, which contains two rate constants. Thus, the dynamic phase behavior of this system was examined for the first time according to these two rate constants. The following important conclusions were obtained. (1) We observed that only the *p*, *i* , and *i+p* phases were present in the system when the PPM was used. (2) We found that as the values of k_2 rate constant increased, the system rapidly relaxed into the *p*, *i* , and *i+p* phases. (3) We obsered that the system contains a special dynamic critical point, such as a dynamic double critical endpoint. (4) When we compared our DPDs with some dynamic theoretical studies of different mixed and pure Ising ferrimagnetic systems, we observed that they were in good agreement. Finally, we hope that our present theoretical work sheds light on theoretical condensed matter physicists or statistical physicists to continue to investigate DPTs and DPDs in different systems within the PPM.

Conflict of interest

The authors report no conflicts of interest in this work.

References

[1] Stanica N., Stager C. V., Cimpoesu M., Andruh M., Synthesis and magnetic properties a of new oxalato-bridged heterotrinuclear complex, $[NiCr_2$ (bipy)$_2$ (μ-$C_2O_4)_2(C_2O_4)_2$ $(H_2O)_2$ $].H_2O$. A rare case of antiferromagnetic coupling between Cr(III) and Ni(II) ions, *Polyhedron 17* (1998) 1787-1789.

[2] Kantar E., Ertaş M., Frequency-Dependent Dynamic Phase Diagrams in Ising System with Fe_4N Structure, *Journal of Superconductivity and Novel Magnetism 29* (2016) 2319-2326.

[3] Numata Y., Inoue K., Baranov N., Field-induced ferrimagnetic state in a molecule-based magnet consisting of a Co (II) ion and a chiral triplet bis(nitroxide) radical, Kurmoo M., Kikuchi K., *Journal of the AmericanNChemical Society 129* (2007) 9902-9909.

[4] Jiang W., Wei G.-z, Zhang Z.-d,Tricritical behavior and magnetic properties for a mixed spin-1 and spin-3/2 transverse Ising model with a crystal field, *Phys. Rev. B 68* (2003) 134432.

[5] Madani M., Gaye A., El Bouziani M., Migdal–Kadanoff solution of the mixed spin-1 and spin-3/2 Blume–Capel model with different single-ion anisotropies, Alrajhi A., *Physica A 437* (2015) 396-404.

[6] Htoutou K., Oubelkacem A., Benhouria Y., Htoutou K., Oubelkacem A., Benhouria Y., Essaoudi I., Ainane A., Ahuja R., The Magnetic Properties of the Mixed Ferrimagnetic Ising System with Random Crystal Field, *Journal of Superconductivity and Novel Magnetism, 30* (2017) 1247-1256.

[7] Motlagh H. N., Rezaei G., Monte Carlo simulation of magnetic properties of mixed spin (3/2, 1) ferromagnetic and ferrimagnetic disordered binary alloys with amorphous structure, *J. Magn. Magn. Mater., 445* (2018) 26-36.

[8] Lafhal A., El Antari A., Hachem N., Al-Rajhi A., Aharrouch R., Saadi H., Madani M., El Bouziani M., Renormalization Group Study of the Mixed Spin-1 and Spin-3/2 Blume-Emery-Griffiths Model with Attractive Biquadratic Coupling, *International Journal of Theoretical Physics, 59* (2020) 1165-1178.

[9] Zaim A., Kerouad M., Monte Carlo simulation of the compensation and critical behaviors of a ferrimagnetic core/shell nanoparticle Ising model, *Physica A, 389* (2010) 3435-3442.

[10] Feraoun A., Kerouad M., The mixed spin-(1,3/2) Ising nanowire with core/inter-shell/outer-shell morphology, *Applied Physics A-Materials Science & Processing, 124* (2018) 124:735.

[11] Vatansever E., Polat H., Monte Carlo investigation of a spherical ferrimagnetic core–shell nanoparticle under a time dependent magnetic field, *J. Magn. Magn. Mater., 343* (2013) 221-227.

[12] Yang M., Wang W., Li Bo-chen, Wu H. J., Yang Shao-qing, Yang J., Magnetic properties of an Ising ladder-like graphene nanoribbon by using Monte Carlo method, *Physica A, 539* (2020) 122932.

[13] Keskin M., Kantar E., Canko O., Kinetics of a mixed spin-1 and spin-3/2 Ising system under a time-dependent oscillating magnetic field, *Phys. Rev. E, 77* (2008) 051130.

[14] Keskin M., Kantar E., Dynamic compensation temperatures in a mixed spin-1 and spin-3/2 Ising system under a time-dependent oscillating magnetic field, *J. Magn. Magn. Mater., 322* (2010) 2789-2796.

[15] Shi X., Qi Y., Existence of a dynamic compensation temperature of the mixed spin-1 and spin-3/2 Ising model within the effective-field theory, *Physica A, 430* (2015) 93-100.

[16] Ertaş M., Keskin M., Dynamic hysteresis features in a two-dimensional mixed Ising system, *Phys. Letts. A, 379* (2015) 1576-1583.

[17] Benhouria Y., Oubelkacem A., Essaoudi I., Ainane A., Ahuja R., Dynamic Magnetic Properties of a Mixed Spin Ising Double-Walled Ferromagnetic Nanotubes: A Dynamic Monte Carlo Study, *Journal of Superconductivity and Novel Magnetism, 30* (2017) 839-844.

[18] Kikuchi R., The Path Probability Method, *Progress of Theoretical Physics Supplement,* 3 (1966) 1–64.

[19] Gençaslan M., Keskin M., Dynamic magnetic hysteresis loop features of a mixed spin (1/2, 1) Ising system on a hexagonal lattice using path probability method, *Modern Phys. Letters, B 35* (2021) 2150221.

[20] Gençaslan M., Keskin M., Influences of the interaction parameters on the dynamic hysteresis of a mixed spin (1/2, 3/2) Ising model under the presence of an oscillating magnetic field, *Int. J. Modern Phys., B 35* (2021) 2150217.

[21] Gençaslan M., Keskin M., Dynamic hysteresis features of a mixed spin (1/2,3/2) Ising system within the path probability method, *Phase Transitions, 95* (2022) 372-386.

[22] Gençaslan M., Keskin M., Dynamic magnetic hysteresis features of a mixed spin (2, 5/2) Ising system on a hexagonal lattice under an oscillating magnetic field within the path probability method, *Int. J. Modern Phys. B, 38* (2024) 2450198.

[23] Gençaslan M., AWWADEE A. M. K., Effect of Cooling Rate on Dynamic Magnetic Hysteresis Loop Behaviors of Magnetic Materials by Using as a Model Mixed Spin (1, 3/2) Ising System Under an Oscillating Magnetic Field, *Journal of Superconductivity and Novel Magnetism, 37* (2024) 1105-1117.

[24] AWWADEE A. M. K., Dynamic Magnetic Properties of a Mixed Spin (1, 3/2) Ferrimagnetic Ising System in an Oscilating Magnetic Field Within the Path Probability Method, *M. Sc. Thesis*, Erciyes University (2024), Kayseri, Türkiye.

[25] İnce O., Gençaslan M., Keskin M., Magnetic features and compensation behaviors of a mixed spin (1/2, 1) Ising ferrimagnetic system on a hexagonal lattice, *Physica A, 583* (2021) 126270.

[26] Gençaslan M., Keskin M., Dynamic magnetic properties of the mixed spin (1/2, 3/2) Ising system in the presence of magnetic field within the path probability method, *Physica A, 559* (2020) 125013.

[27] İnce O., Gençaslan M., Keskin M., Dynamic phase of transitions of the mixed spin (1/2, 3/2) Ising model in the presence of a time-varying magnetic field by using the path probability method, *Phys. Letters A, 390* (2021) 127107.

[28] Alhameri M. F. İ., Dynamic phase transitions and compensation behaviors in a mixed spin (1/2,3/2) Ising model on a hexagonal lattice by path probability method, Gençaslan M., Keskin M., *Indian J. Physics, 96* (2022) 3775-3786.

[29] Gençaslan M., Keskin M., Nonequlibrium magnetic features in a mixed spin (2, 5/2) Ising system driven by the external oscillating magnetic field by path probability method, *Physica Scripta, 97* (2022) 085803.

[30] Gençaslan M., Özlü M., Keskin M., Dynamic Magnetic Features of a Mixed-Spin-2 and Spin-5/2 Ising Ferrimagnetic System under a Time-Dependent Oscillating Magnetic Field: Path Probability Method Approach, *Phys. Status Solidi, B 260* (2023) 2200425.

[31] Chakrabarti K., Acharyya M., Dynamic transitions and hysteresis, *Rev. Mod. Phys., 71* (1999) 847-859.

[32] Yunus Ç., Renklioğlu B., Keskin M., Stepwise positional-orientational order and the multicritical-multistructural global phase diagram of the *s*=3/2 Ising model from renormalization-group theory, Berker A. N., *Phys. Rev. E, 93* (2016) 062113.

[33] Deviren B., Keskin M., Canko O., Kinetics of a mixed spin-1/2 and spin-3/2 Ising ferrimagnetic model, *J. Magn. Magn. Mater., 321* (2009) 458-466.

[34] Ertaş M., Keskin M., Dynamic magnetic behavior of the mixed spin (2, 5/2) Ising system with antiferromagnetic/antiferromagnetic interactions on a bilayer square lattice, *Chin. Phys. B, 22* (2013) 120507.

[35] Ertaş M., Deviren B., Nonequilibrium magnetic properties in a two-dimensional kinetic mixed Ising system within the effective-field theory and Glauber-type stochastic dynamics approach, Keskin M., *Phys. Rev. E, 86* (2012) 051110.

[36] Deviren Ş. A., Deviren B., Dynamic magnetic properties of a mixed-spin (1, 3/2) Ising nanotube: a dynamic mean-field study, *Eur. Phys. J. Plus, 137* (2022) 1067.

[37] Ertaş M., Deviren B., Dynamic magnetic properties of multilayer mixed spin-1 and spin-3/2 Ising model, *Eur. Phys. J. Plus, 137 (2022)* 1031.